UNCLASSIFIED

AD NUMBER
AD424152
LIMITATION CHANGES

TO:

Approved for public release; distribution is unlimited.

FROM:

Distribution authorized to U.S. Gov't. agencies and their contractors; Administrative/Operational Use; 21 NOV 1963. Other requests shall be referred to Office of Naval Research, Arlington, VA 22203.

AUTHORITY

ONR ltr 4 May 1977

THIS PAGE IS UNCLASSIFIED

THIS REPORT HAS BEEN DELIMITED
AND CLEARED FOR PUBLIC RELEASE
UNDER DOD DIRECTIVE 5200.20 AND
NO RESTRICTIONS ARE IMPOSED UPON
ITS USE AND DISCLOSURE,

DISTRIBUTION STATEMENT A

APPROVED FOR PUBLIC RELEASE;
DISTRIBUTION UNLIMITED,

UNCLASSIFIED

AD 424152

DEFENSE DOCUMENTATION CENTER

FOR

SCIENTIFIC AND TECHNICAL INFORMATION

CAMERON STATION, ALEXANDRIA, VIRGINIA

UNCLASSIFIED

Measurement of Fluid Properties for
Magnetoplasmadynamic Power Generators

Second Quarterly Technical Summary Report

(1 August—31 October 1963)

Contract No. Nonr-4104(00)

Order No.: ARPA 420   Project Code No. 3980

Engineering Department Report No. 3632
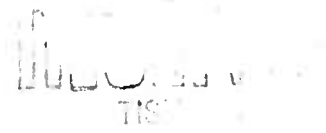
Allison Division

General Motors Corporation

Indianapolis, Indiana

Measurement of Fluid Properties for Magnetoplasmadynamic Power Generators

Second Quarterly Technical Summary Report

(1 August—31 October 1963)

By: R. T. Schneider
    H. E. Wilhelm
    D. L. Tipton
    W. Woerner

Approved: _F.G.Myers_____

     for T. F. Nagey
          Director of Research

FOREWORD

This technical summary report was prepared by the Research Department of the Allison Division of General Motors Corporation. The work reported was accomplished under Contract Nonr-4104(00).

TABLE OF CONTENTS

iii

LIST OF ILLUSTRATIONS

LIST OF TABLES

I. INTRODUCTION

This second Quarterly Technical Summary Report describes the progress made in the period 1 August through October 31. During this period, the construction of the Allison diagnostic MPD device was completed and the first checkout run was made. This report, therefore, deals with the final description of the loop. Most emphasis is laid upon the description of the diagnostic methods, which were prepared for the use on the loop. Therefore, actual test data with the unseeded working fluid will be included in the next quarterly report.

II. RESUME OF PROGRESS

CONSTRUCTION OF CLOSED LOOP DIAGNOSTIC MPD DEVICE

The final assembly of the diagnostic MPD system has been completed. For the first checkout, the tantalum MPD test section was replaced by a stainless steel insert. The tantalum MPD test section itself has been completed and is ready for incorporation into the system.

The system was operated for a total of one hour and then taken apart for inspection of the components. The run with the highest temperature was made at 1000°K. The impurities measured were oxygen with 1.75 ppm and water vapor with 48 ppm.

A sample piece of tantalum was weighed and then installed in the stainless steel insert section for the aforementioned test. It did not show any wear after the test; therefore, more running time must be accumulated before the weight of the lost mass can be determined.

A gas discharge tube was manufactured which can be attached to the insert test section for spectroscopic determination of the impurities. This investigation is scheduled for the next run.

Presently, it is planned to accumulate more running time on the system to get more information on the reliability of the single components. * Following this, the tantalum test section will be incorporated into the system and the measurements with the unseeded working fluid will be completed in the next reporting period.

DEVELOPMENT AND ADAPTION OF DIAGNOSTIC METHODS

Further development of diagnostic methods was accomplished. A part of this work was the subject of an article, "Calculation and Measurement of the Radial Distribution of Line Broadening in a Cesium Plasma," by D. L. Tipton and R. T. Schneider, Applied Spectroscopy 17, 147, 1963. This work is an application of Abel's integral equation on the broadening of a spectrum line to determine the electron density profile of a cylindrical plasma. This method will be applied to find changes in the electron density in the MPD device.

---

*In the meantime, eight hours of running time have been accumulated at 1350°K maximum temperature.

Another part of the work accomplished during the reporting period is described in Spectroscopic Technique for Temperature or Pressure Measurement in Plasmas, by R. T. Schneider, W. Woerner, and H. E. Wilhelm. This paper included as a part of Section IV of this report, describes a new method for spectroscopic temperature measurement. The advantages of the new method are: (1) the transition probabilities need not be known, and (2) the photographic plate need not be calibrated.

THEORETICAL INVESTIGATIONS

Ionization Equilibrium in Magnetic Field

The partition functions for the components of a partially ionized plasma energized with a magnetic field have been calculated on a statistical basis. These allow a complete description of the magnetothermodynamic properties of the plasma. As an application, the ionization equilibrium in a strong magnetic field will be calculated.

Nonequilibrium Ionization in Magnetic Field

Statistical investigations of the properties of a reacting plasma by means of the kinetic equations have been started. As an intermediate application, the electrical and thermal conductivity of seeded plasma will be calculated. Following this, a kinetic nonequilibrium ionization theory will be developed

Results of these investigations will be included in the third quarterly report.

III. THE ALLISON DIAGNOSTIC CLOSED LOOP MPD DEVICE

FINAL ASSEMBLY AND LEAK TESTING

The design of the Allison MPD diagnostic loop was described in the first Quarterly Report, EDR 3511. Therefore, in this report only the final assembly is described and a few minor changes in the design are pointed out. Figure 1 is a schematic of the loop. The changes in this schematic as compared with the schematic presented in EDR 3511 are:

- An additional line was installed to bypass the helium compressor. The reason: to take the compressor (a possible major leak source during the mass-spectrometer leak testing) out of the system. Once the system was made leakproof, the compressor was put back in the system; any new leaks now could be located more easily.
- A new vacuum line was installed for evacuating the bearing housings separately. The narrow clearance precluded a good evacuation through the main vacuum line. Also, the purified helium refill will be made with the same line. Another sampling valve was installed for continuous sampling in the vicinity of the orifice flow meter.
- A bypass line from the MPD test section back to the system was installed to handle the helium cover gas which is used to cool the test section.

Figure 2 depicts the system during assembly; this is a portion of that part of the system which is located inside the building (also, see Figure 1). The following components are shown in Figure 2: charcoal filter, NaK bubblers, magnet, cesium tank, helium bottles.

The part of the system outside the building is shown in Figure 3. Included in Figure 3 are the following components: helium compressor, filter, cesium tank, helium bottles.

Figure 4 is a special view of the coolers. The coolers are sloped so that the cesium can flow back to the helium cesium separator located at the extreme left in Figure 4.

Figure 5 shows the control panel. The location of the controls which are panel mounted is shown on the schematic in Figure 1.

The heater and the magnet are depicted in Figure 6. The hole in the core of the magnet, which gives access for optical observation of the test section, is visible in the center of Figure 6.

After assembly, the system was leak tested using a mass spectrometer leak detector. Only a few small leaks occurred in the system itself. None of the welds had to be redone. Approximately ten medium leaks had to be repaired in the helium compressor. After this was done, the system, with the helium compressor and a stainless steel insert test section in place, could be pumped down to 1×10^{-4} Torr.

FIRST CHECKOUT RUNS

The main purposes of the first checkout runs were to test the heater and to get preliminary information on the impurity level in the system.

Figure 7 shows the heater coil before the first test. Figure 8 shows the same coil after one hour running time with a maximum gas temperature of 1000°K. The tungsten wire has been polished by the high velocity helium gas at those areas where a high temperature was encountered. See Figure 8. A part of the coil looks bright metallic, while before the run the surface of the coil was dark and rough (see Figure 7). Traces of tungsten were evaporated from the coil and condensed on the insulator. This also can be seen when comparing the white insulator, which supports the tungsten coil in Figure 8, with that in Figure 7.

For this preliminary run a boron nitride insulator was used. The boron nitride insulator worked out better than expected. However, for higher gas temperatures thoria will be used to avoid possible damage of the tantalum test section by nitrogen and of the stainless steel coolers by boron. Thoria insulators are on order and will be available for the actual MPD runs. The boron nitride insulator shows some damages. Small pieces broke off, probably due to the thermal shock (see Figure 8). The damaged areas have no plated tungsten traces. That means that the damage occurred after the current was shut off. Therefore, for future runs, provisions will be made not only to increase the current slowly, but also to decrease the current very gradually.

During the first runs water vapor and oxygen content were monitored. The water vapor was continuously sampled by a Beckman Electrolytic Hygrometer. The initial water vapor content in the loop was well above 1000 ppm. It was lowered first by purging, then by circulating through the helium purification system. The best value which could be obtained was 48 ppm. The water vapor of the helium, which comes from the bottles, is 11 ppm. The additional water vapor content in the system probably comes from the stainless steel walls in the system.
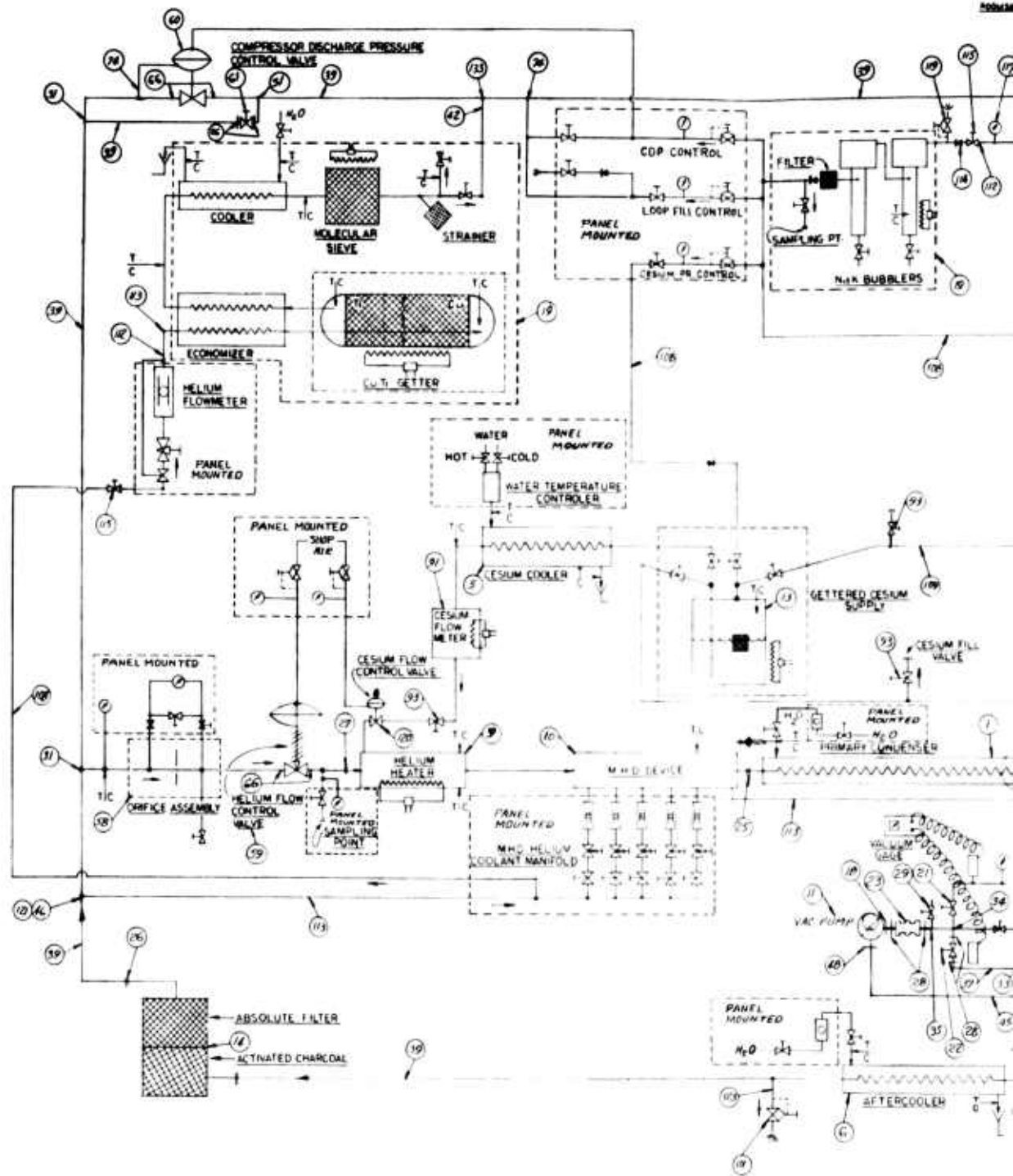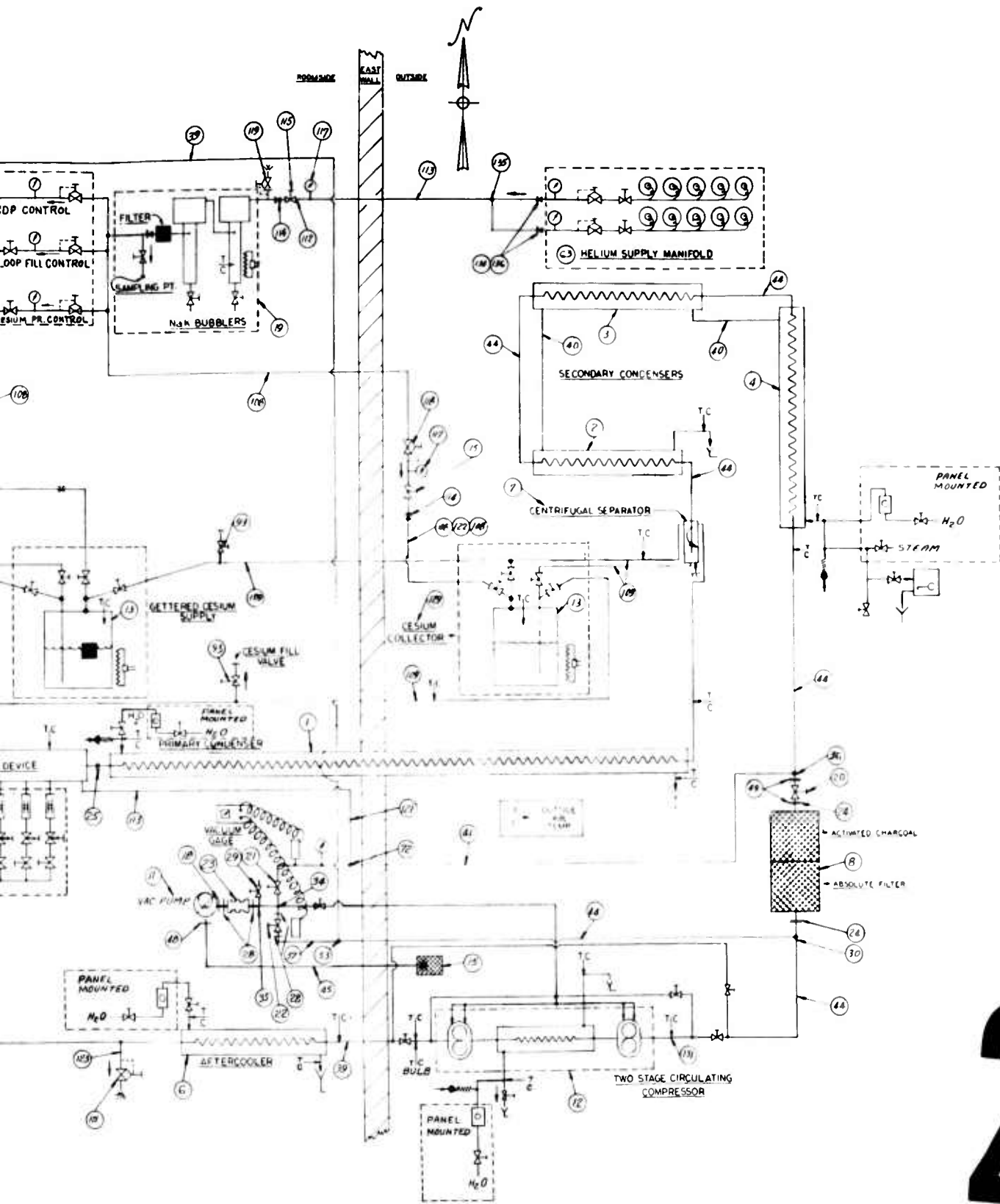
Figure 1.

Figure 1. Final form of the schematic of the Allison closed-loop MPD diagnostic device

7

1. Charcoal filter
2. NaK bubbler
3. Magnet
4. Cesium tank
5. Vacuum pump

Figure 2. A portion of the system located inside the building—during assembly
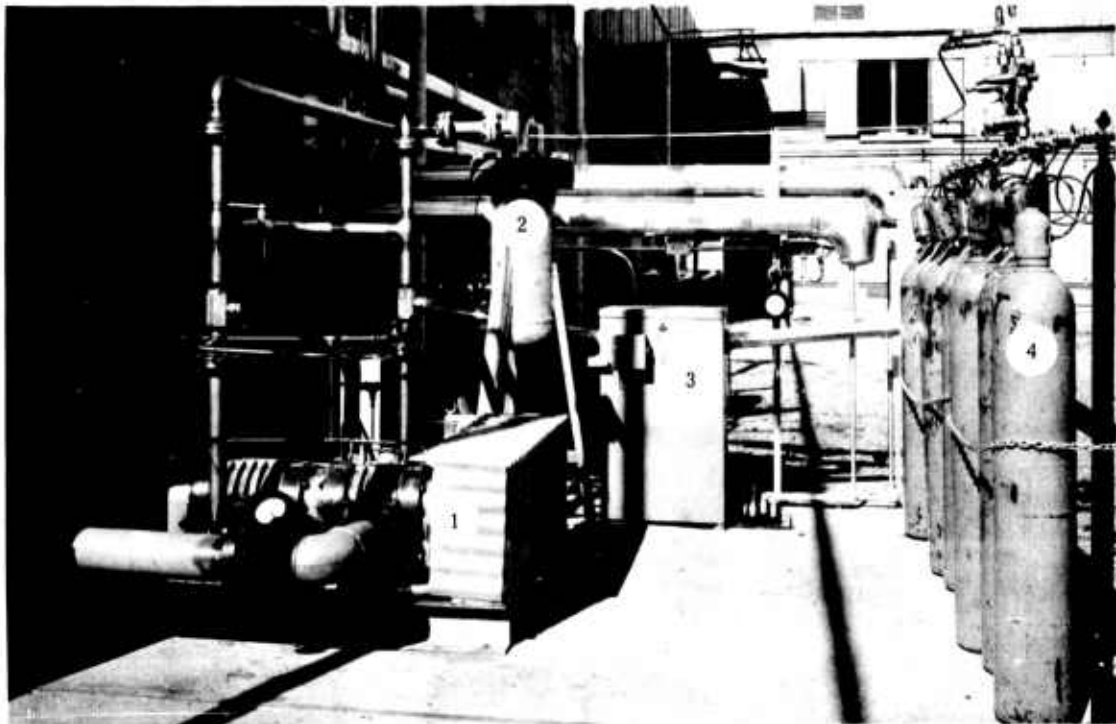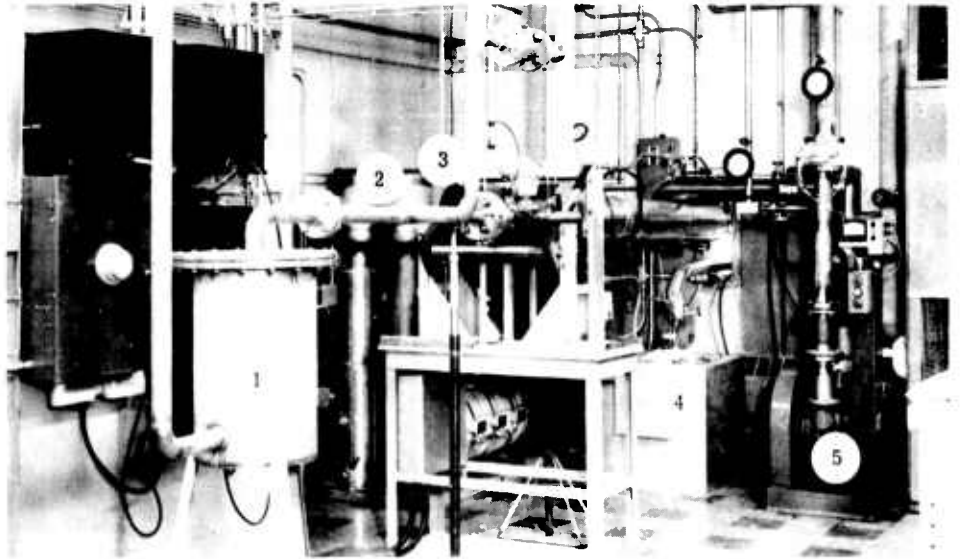
1. Helium compressor
2. Filter
3. Cesium tank
4. Helium bottles

Figure 3. The part of the system located outside the building
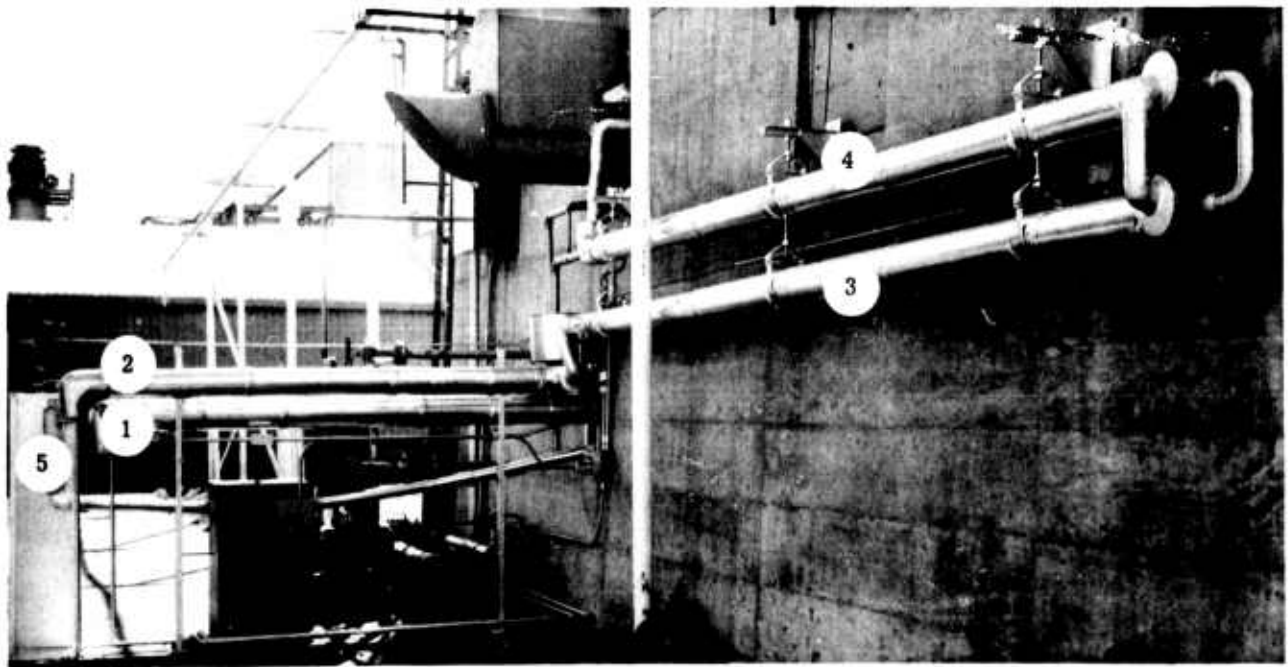
1. Primary condenser   3. Second aftercooler   5. He - Cs separator

2. First aftercooler   4. Third aftercooler

Figure 4. Cooling system
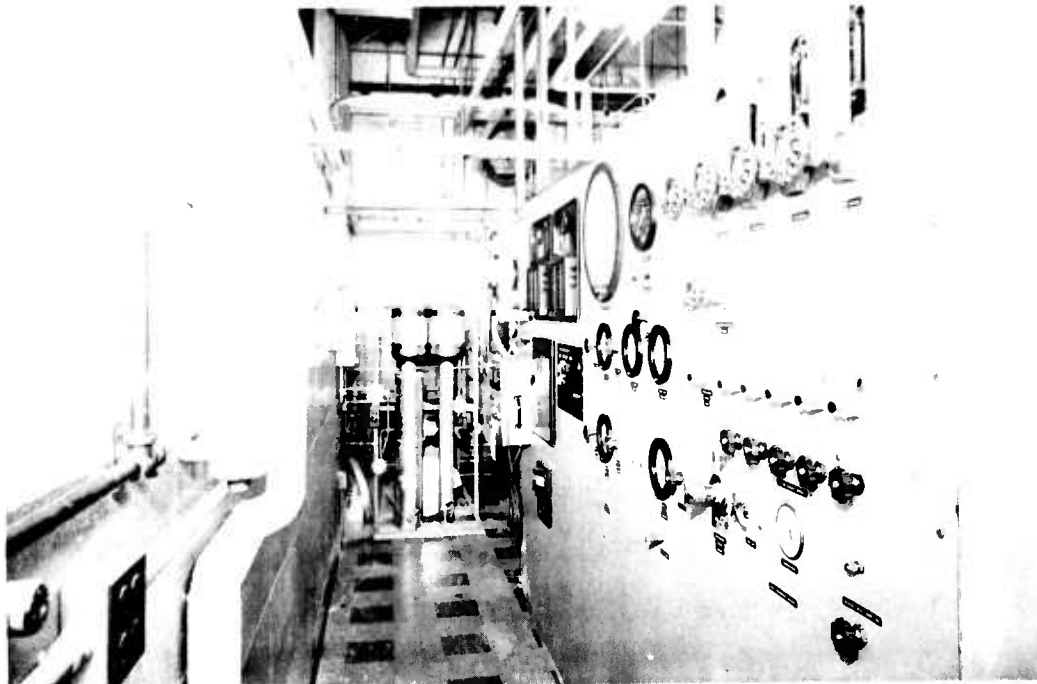
Figure 5. Control panel for the system
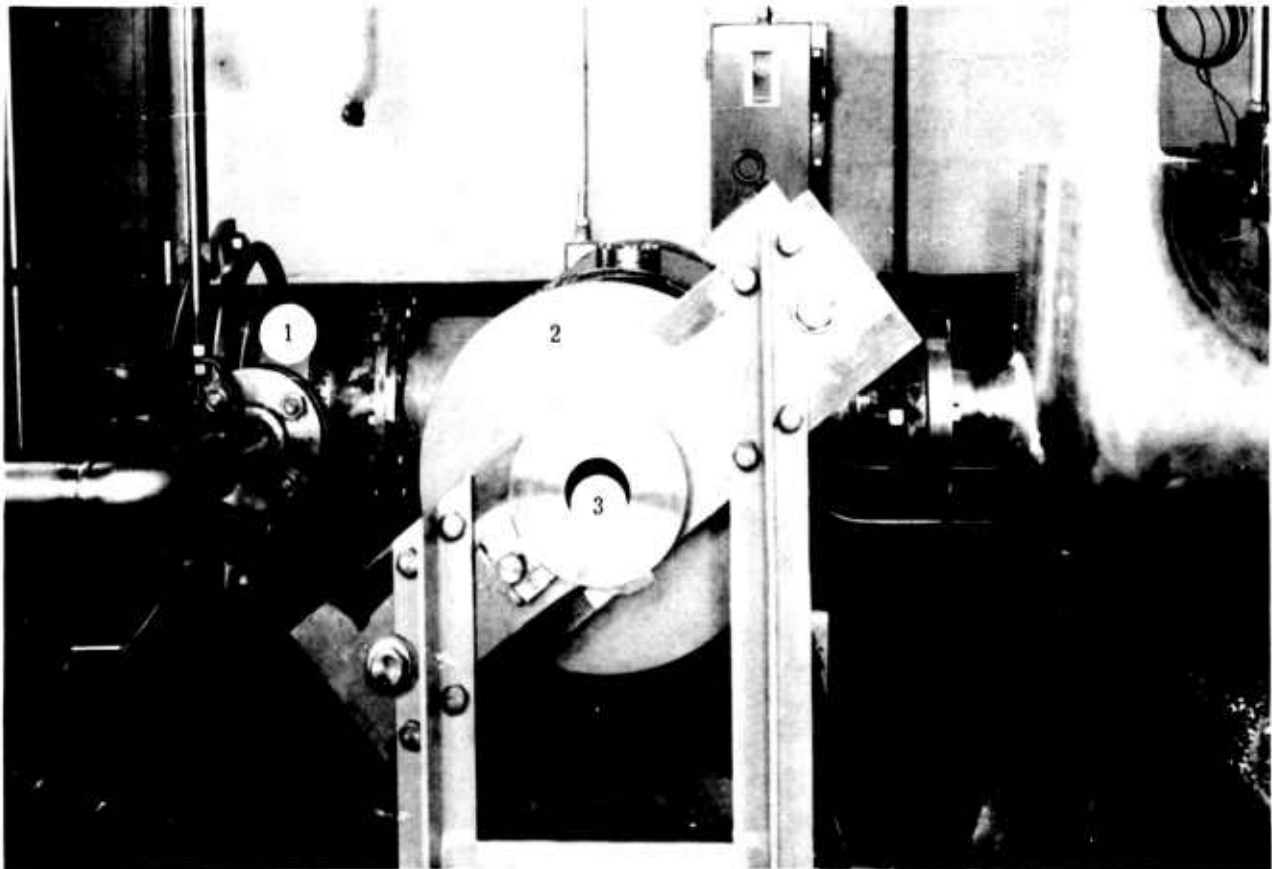
| 1. Heater | 2. Magnet | 3. Observation hole |

Figure 6. Heater and magnet assembly

The oxygen content was continuously sampled by an oxygen analyzer (Lockwood and McLorie). The best value obtained was 1.75 ppm. The content of the bottle helium was 1.5 ppm.

The oxygen content should not cause any trouble; however, the water vapor content should be decreased. Efforts are being made to do this.

Figure 9 shows the MPD device with the stainless steel insert during operation at 1350°K.

A summary of the first runs follows:

1. The minimum mass flow for safe heater operation has been determined to be 3 gr/sec.
2. The heater operated satisfactorily to at least 1400°K gas temperature.
3. The tantalum sample piece did not show any wear at the described operation conditions.

11
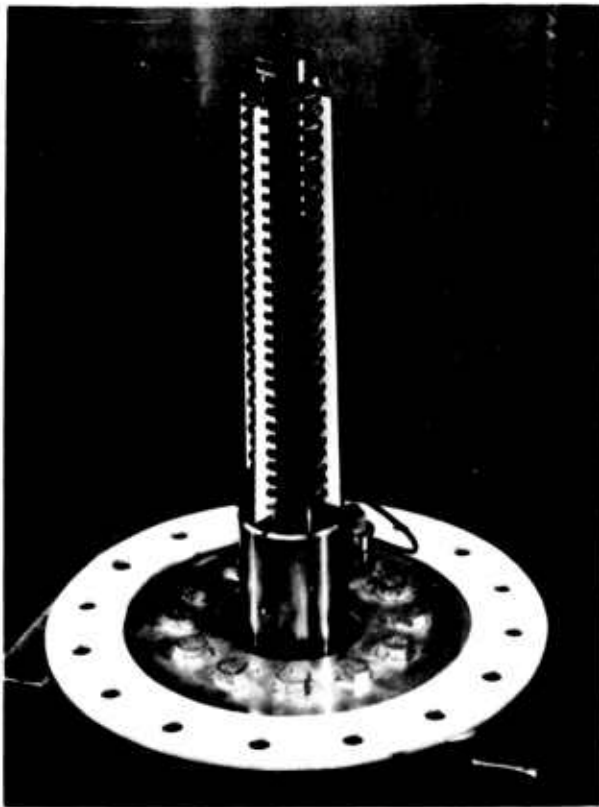
Figure 7.   Tungsten coil of high temperature resistance heater before the first run
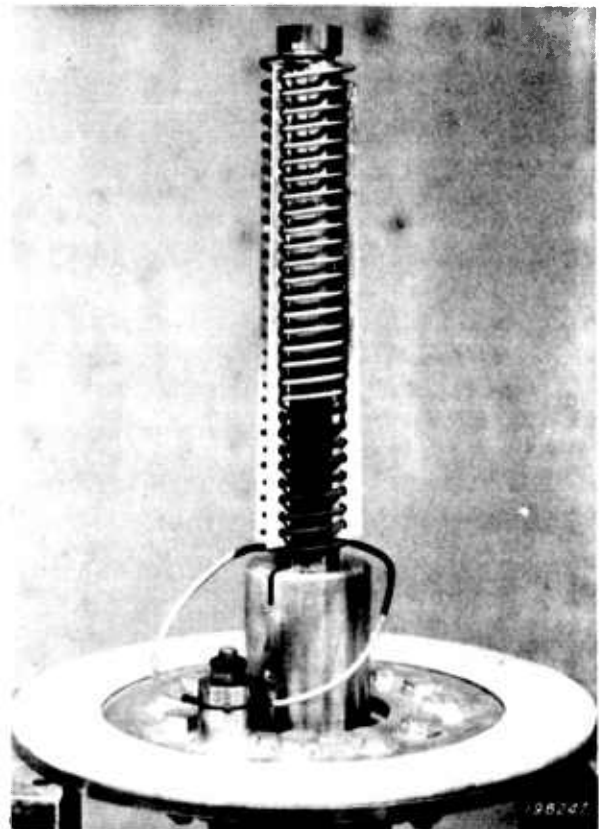
Figure 8.   Tungsten coil of high temperature resistance heater after one hour running time
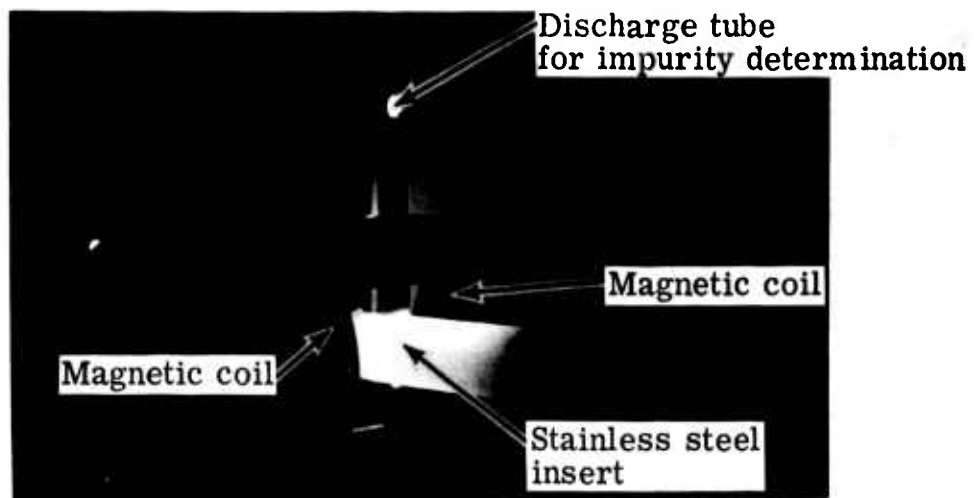
Figure 9.   MPD-device with stainless steel insert during operation at 1350°K

IV. DIAGNOSTIC METHODS

Spectroscopic Technique for Temperature or Pressure
Measurement in Plasmas

INTRODUCTION

Spectroscopic methods for measurement of temperature or pressure have the advantage that they do not change the conditions of the plasma. They are, therefore, very useful for application on small-volume plasma devices (e.g., MHD power generators and thermionic energy converters).

Most of the spectroscopic temperature measurement methods apply, in one way or the other, the basic relation for the intensity of spectral lines. Assuming optically thin plasma and Boltzmann distribution of the excited states of the atom, the intensity of a spectral line resulting from a transition $m \rightarrow n$ is given by

$$I_n^m = A_n^m \, g_m \, h \, \nu_n^m \, \frac{n \, (P, T)}{u \, (T)} \, e^{-E_m/kT} \times \ell \tag{1}$$

where

A_n^m = transition probability
g_m = statistical weight
h = Planck's constant
ν_n^m = line frequency
n = $n(P, T)$ = atom density
u = $u(T)$ = partition function
E_m = excitation energy
k = Boltzmann constant
T = Temperature in °K
ℓ = geometric length

By means of Equation (1), the temperature can be determined from the experimentally observed absolute line intensity when the transition probability and the atom density are known. A shortcoming of this method is that the photographic emulsion has to be calibrated.

13

The requirement for an absolute calibration can be avoided by determining the temperature from the intensity ratio of different spectral lines (Ornstein[1]*). For the transitions $m \rightarrow n$ and $p \rightarrow q$, this intensity ratio is given by

$$\frac{I_n^m}{I_q^p} = \frac{A_n^m g_m}{A_q^p g_p} \cdot \frac{\nu_n^m}{\nu_q^p} \left[e^{- (E_m - E_p)/kT} \right] \tag{2}$$

In this case, only a relative calibration is necessary. Furthermore, only relative transition probabilities have to be known, for which, in general, more accurate values are available than for absolute transition probabilities.

Relative temperature measurement is possible, finally, without knowledge of transition probabilities (Hoermann[2] and Maecker[3]). In this method, use is made of the relation for the intensity ratio of one and the same spectral line at different temperatures:

$$\frac{I_n^m (T_1)}{I_n^m (T_2)} = \frac{n (P, T_1) U (T_2)}{n (P, T_2) U (T_1)} e^{-\left[\frac{E_m}{k} \left(\frac{1}{T_1} - \frac{1}{T_2} \right) \right]} \tag{3}$$

Equation (3) allows measurement of relative spatial temperature changes and absolute measurement of temperature profiles, assuming the temperature is known at one point. It is also recognized that the sensitivity of the emulsion need not be known because intensities of the same wavelength are compared.

If in the plasma under consideration a spectral line has maximum intensity in a region that is known not to contain the maximum temperature, this line intensity maximum is due to the fact that, in this case, the maximum radiation intensity is already reached at a temperature below the temperature maximum. The temperature corresponding to this maximum of radiation intensity can be calculated by the method of Fowler and Milne[4] and used as a reference temperature in Equation (3). Larenz[5] and Bartels[6] used this method to determine absolute temperature profiles in arcs.

In the following paragraphs, a similar method is described which, however, does not require the detection of the maximum of intensity versus temperature curve of a spectrum line. This method can be used for plasma temperature determination when the total pressure of the plasma is known, or for pressure determination when the temperature is known.

*Superscripts denote references presented in Section VI.

METHOD

The derivation of the basic equations for the new method is carried through for a plasma consisting of two different gas species. As an application in particular, an alkali-seeded noble gas plasma is considered. For the calculation of the particle densities in the plasma, the validity of the equation of state for perfect gases and of Saha's equation is assumed. In the latter, a Boltzmann distribution of the excited atomic states also is assumed. It is remarkable, however, that these assumptions place no restriction on the method itself which can also be extended to plasmas deviating strongly from thermodynamic equilibrium.

Let the densities of the neutrals and ions be designated by n_A, n_{A+} for the first gas species, and by n_B, n_{B+} for the second gas species. The total electron density in the plasma is n_-. With these designations the Saha equations describing the ionization equilibrium in the two-gas plasma are:

$$\frac{n_{A+}\, n_-}{n_A} = \phi_A, \quad \phi_A \equiv 2 \left(\frac{2\pi m_e}{h^2}\right)^{3/2} \frac{u_{A+}}{u_A} (kT)^{3/2}\, e^{-\frac{W_A}{kT}} \tag{4}$$

$$\frac{n_{B+}\, n_-}{n_B} = \phi_B, \quad \phi_B \equiv 2 \left(\frac{2\pi m_e}{h^2}\right)^{3/2} \frac{u_{B+}}{u_B} (kT)^{3/2}\, e^{-\frac{W_B}{kT}} \tag{5}$$

where

W_A = effective ionization energy of the neutrals A

W_B = effective ionization energy of the neutrals B

$$u_A = \sum_{s=0}^{\infty} g_{As}\, e^{-\left(\frac{x_{As}}{kT}\right)} \Bigg\rbrack \quad \text{neutrals A}$$

partition functions of the

$$u_{A+} = \sum_{s=0}^{\infty} g_{As}^+\, e^{-\left(\frac{x_{As}^+}{kT}\right)} \Bigg\rbrack \quad \text{ions A+}$$

$$u_B = \sum_{s=0}^{\infty} g_{Bs}\, e^{-\left(\frac{x_{Bs}}{kT}\right)} \quad \text{neutrals B}$$

$$\left. \begin{array}{c} \end{array} \right\} \quad \text{partition function of the}$$

$$u_{B+} = \sum_{s=0}^{\infty} g_{Bs}^{+}\, e^{-\left(\frac{x_{Bs}^{+}}{kT}\right)} \quad \text{ions B+}$$

(6)

$g_{As},\ g_{Bs},\ g_{As}^{+},\ g_{Bs}^{+}$ = statistical weights of the intrinsic states of the
neutrals and ions

$x_{As},\ x_{Bs},\ x_{As}^{+},\ x_{Bs}^{+}$ = excitation energies of the intrinsic
states of the neutrals and ions

The considered ionization equilibrium refers to a temperature range and mixing proportions for which double and higher multi-ionizations can be neglected quantitatively. Equations (4-5) have to be supplemented by the equation of state:

$$P = (n_A + n_{A+} + n_B + n_{B+} + n_-)kT \quad \text{(equal temperature of the components assumed)} \quad (7)$$

the condition for electrical neutrality:

$$n_- = n_{A+} + n_{B+} \tag{8}$$

and the definition equation for the mixing proportion:

$$a = \frac{n_A + n_{A+}}{n_B + n_{B+}} \tag{9}$$

From Equations (4) through (9), the particle densities can be calculated as function of temperature, T, total pressure, P, and mixing proportion, a. It results that the electron density is given as the positive real root of the cubic

$$n_-^3 + n_-^2 \left[\phi_A + \phi_B + \frac{a\phi_A + \phi_B}{1+a} \right] +$$

$$n_- \left[2\phi_A \phi_B - \frac{a\phi_A + \phi_B}{1+a} \cdot \frac{P}{kT} \right] - \phi_A \phi_B \frac{P}{kT} = 0 \tag{10}$$

The other particle densities can be reduced to the electron density:

$$n_{A+} = a\, n_- \frac{\phi_A}{\phi_B} \left(\frac{n_- + \phi_B}{n_- + \phi_A}\right) \cdot \left[1 + a\, \frac{\phi_A}{\phi_B}\left(\frac{n_- + \phi_B}{n_- + \phi_A}\right)\right]^{-1} \qquad (11)$$

$$n_{B+} = n_- \cdot \left[1 + a\, \frac{\phi_A}{\phi_B}\left(\frac{n_- + \phi_B}{n_- + \phi_A}\right)\right]^{-1} \qquad (12)$$

$$n_A = a\, n_- \frac{n_-}{\phi_B}\left(\frac{n_- + \phi_B}{n + \phi_A}\right) \cdot \left[1 + a\frac{\phi_A}{\phi_B}\left(\frac{n_- + \phi_B}{n_- + \phi_A}\right)\right]^{-1} \qquad (13)$$

$$n_B = n_- \frac{n_-}{\phi_B} \cdot \left[1 + a\, \frac{\phi_A}{\phi_B}\left(\frac{n_- + \phi_B}{n_- + \phi_A}\right)\right]^{-1} \qquad (14)$$

The further relations are equal in form for both neutral species. For convenience, the indices A and B will, therefore, be omitted.

By means of Equations (10), (13), and (14), the following expression, consisting of particle densities and partition functions of one of the neutral species, can be calculated as function of pressure P and temperature T_1, with a as parameter:

$$b = \log\left[\frac{n(P,\ T_1)\ u(T_2)}{n(P,\ T_2)\ u(T_1)}\right], \qquad T_2 \equiv \frac{T_1}{1 - aT_1} \qquad (15)$$

Physically, the expression b refers to two points in the plasma with different temperatures, T_1 and T_2. The pressure, P, is presumed constant. This is valid for many applications where exterior force fields are negligible [otherwise, the substitutions $(P,\ T_1) \to (P_1, T_1)$, $(P, T_2) \to (P_2, T_2)$ have to be made in Equation (15)]. The expression b and the temperature parameter,

$$a = \frac{1}{T_1} - \frac{1}{T_2} \qquad (16)$$

are experimental observables and can be measured by spectroscopic methods. Thus, by inserting the experimentally determined a- and b- values into Equation (15), an implicit equation in P and T_1 is obtained. From this, either T_1, when P is known, or P, when T_1 is known, can be calculated numerically.

Let us now explain how the fundamental expression b and the temperature parameter a are determined spectroscopically.

Assuming a distribution according to Boltzmann statistics, the number density of atoms in excited state m is given by

$$n_m = \frac{n(P, T)}{u(T)} g_m e^{-E_m/kT} \tag{17}$$

For the ratio of number densities of excited atoms in the state m in the same plasma at different temperatures, T_1 and T_2, it follows that

$$\frac{n_m(T_1)}{n_m(T_2)} = \frac{n(P, T_1)}{n(P, T_2)} \cdot \frac{u(T_2)}{u(T_1)} e^{-\frac{E_m}{k}\left(\frac{1}{T_1} - \frac{1}{T_2}\right)} \tag{18}$$

According to Equations (1) and (18), the intensity ratio of two spectral lines measured at two points with different temperatures, T_1 and T_2, in the same plasma and resulting from one and the same transition, $m \rightarrow n$, is given by

$$\frac{I_n^m(T_1)}{I_n^m(T_2)} = \frac{n(P, T_1)}{n(P, T_2)} \cdot \frac{u(T_2)}{u(T_1)} e^{-\frac{E_m}{k}\left(\frac{1}{T_1} - \frac{1}{T_2}\right)} \tag{19}$$

Dividing Equation (19) by the corresponding equation for the transition $p \rightarrow q$, the following relation is obtained:

$$\frac{I_n^m(T_1)}{I_n^m(T_2)} \cdot \left[\frac{I_q^p(T_1)}{I_q^p(T_2)}\right]^{-1} = e^{-\frac{(E_m - E_p)}{k}\left(\frac{1}{T_1} - \frac{1}{T_2}\right)} \tag{20}$$

By introducing the temperature parameter a [see Equation (16)] and the decadic logarithms of the intensity ratios:

$$\bullet \quad \Delta Y_n^m = \log \frac{I_n^m(T_1)}{I_n^m(T_2)}, \, \Delta Y_q^p = \log \frac{I_q^p(T_1)}{I_q^p(T_2)} \tag{21}$$

Equation (20) can be rewritten in the form:

$$\bullet \quad a = \frac{k \ln 10}{E_p - E_m} \left[\Delta Y_n^m - \Delta Y_q^p\right] \tag{22}$$

18

This relation permits the temperature parameter a to be determined spectroscopically by measuring the decadic logarithms of the intensity ratios defined in Equation (21) for two spectrum lines. Similarly, by introducing the fundamental expression b [see Equation (15)], Equation (19) can be rewritten in the form:

$$● \quad b = \Delta Y_n^m + \frac{E_m}{k \ln 10} \cdot a \qquad (23)$$

This relation, Equation (23), shows, finally, that the fundamental expression b can be determined experimentally from the measured ΔY_n^m - and a- value. The demonstrated method works without knowing transition probabilities. According to Equations (22) and (23), only the two excitation energies, E_m and E_p, have to be known. The $\Delta Y_{n,q}^{m,p}$ compares intensities at the same wavelength; therefore, the dependence of sensitivity from the wavelength does not have to be known.

Usually, in most plasmas the change in photographic density is much greater due to the change in sensitivity of the photographic plate rather than to the change in radiation from the plasma— using, for example, the line ratio technique (Equation 2). It is, therefore, very desirable to remove the source of error.

As already mentioned, by inserting the experimentally obtained a- and b- value into Equation (15), either T_1 can be calculated if P is known, or P can be calculated if T_1 is known. In practical applications, however, it is suitable to make use of a graphic representation. For this, the theoretical curves representing the fundamental expression

$$b = \log \left[\frac{n(P, \ T_1) \cdot u\left(\frac{T_1}{1 - aT_1}\right)}{n\left(P, \frac{T_1}{1 - aT_1}\right) \cdot u(T_1)} \right] \qquad (24)$$

are drawn as function of T_1 and P, respectively (abscissa), where, in the first case, a and P and in the second case, a and T_1 are treated as parameters. From these two parametric curve representations, the unknown temperature, T_1, or pressure, P, respectively, are read as follows. The experimental a- value and the second parameter, P or T_1, respectively, designate the theoretical b- curve that applies. The experimental b- value gives a definite point on this curve. The abscissa of this point represents the unknown observable.

As an application, the theoretical b- value has been calculated as a function of temperature T_1 = 1000 to 6000°K for a cesium-seeded helium plasma—with a pressure of P = 1 atmosphere, the seeding ratio $\alpha = 10^{-2}$, and a number of a- values as parameters. The ionization potentials of cesium and helium were taken as

$$W_{Cs} = 3.893 \text{ eV}, \ W_{He} = 24.580 \text{ eV} \tag{25}$$

The depression of the ionization potentials due to the electrostatic microfield and the Debye polarization representing under the given conditions a small correction[7]

$$\Delta W = 0.67 \times 10^{-6} n_-^{1/3} + 0.37 \times 10^{-7} \left(\frac{n_-}{T}\right)^{1/2} \text{ eV}, \tag{26}$$

was considered by means of a successive approximation.

The numerical results are represented graphically in Figure 10 for a helium-cesium mixture with a seeding ratio $\alpha = 10^{-2}$. Curves for pure cesium and pure helium and other seeding ratios will be included in a later report.

ERROR CONSIDERATION

The accuracy of the method depends noticeably on the compared temperatures T_1, T_2 in the plasma—i.e., also on the temperature parameter $a = \frac{1}{T_1} - \frac{1}{T_2}$—and the pressure P. With respect to temperature measurement, this is recognized easily from the theoretical b- curves (Figure 10) by estimating graphically the error ΔT_1 due to certain assumed experimental errors, Δa and Δb, over the whole range of T_1, a, and b. To see how the error in the measuring result depends (in principle) on the respective values of T_1, P, and a, an analytical representation is given for a simple plasma consisting of one kind of atomic and ionic species. In this case, the neutral density is given by [see Equations (4), (7), and (8)]:

$$n(P, \ T) = 2 \left[\frac{P}{2kT} + \phi(T) \left(1 - \sqrt{1 + \frac{P}{\phi(T) kT}}\right)\right]$$

$$\phi(T) = 2\left(\frac{2\pi m_e}{h^2}\right)^{3/2} \frac{u_+}{u} (kT)^{3/2} e^{-W/kT} \tag{27}$$

20
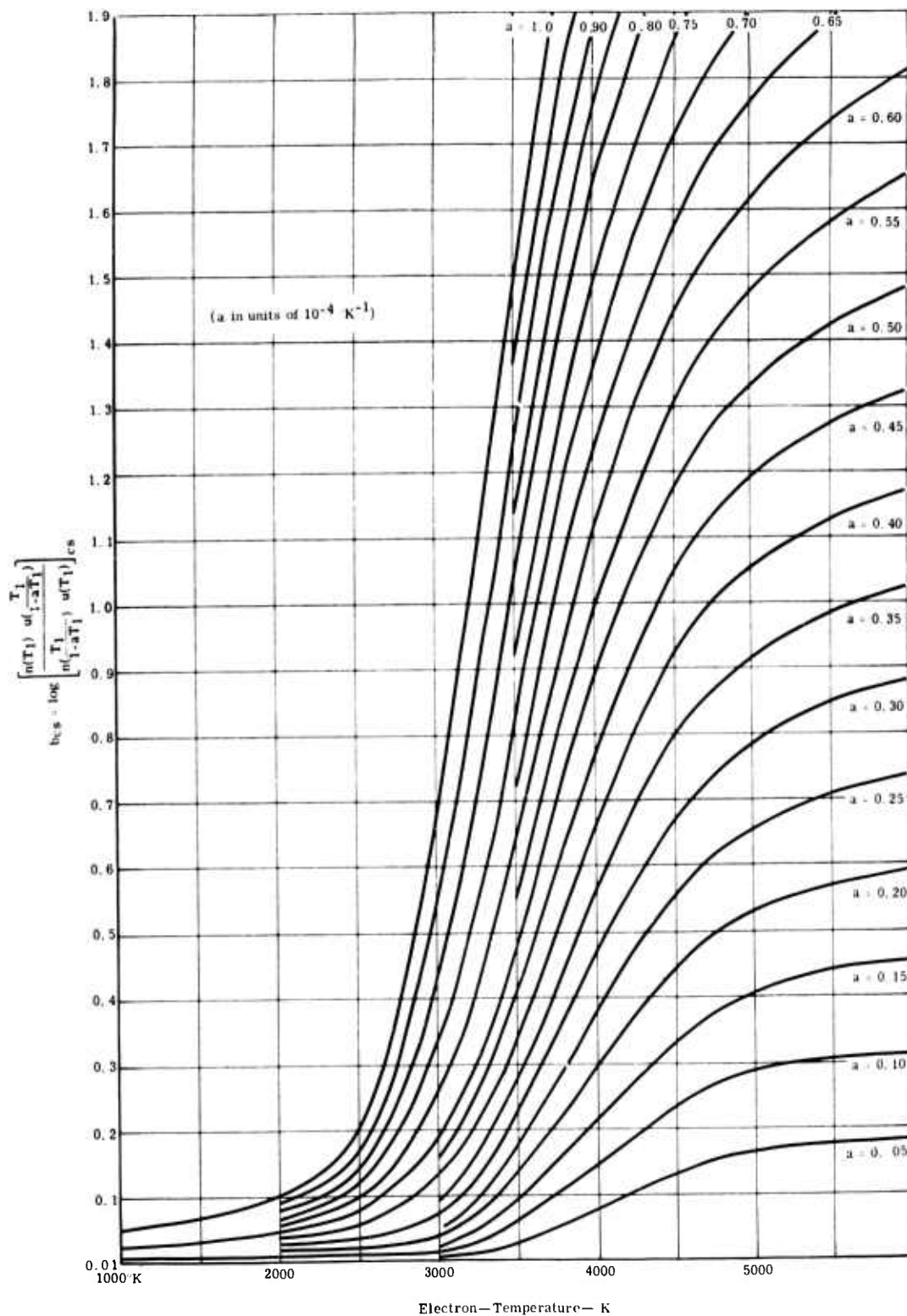
Figure 10. Theoretical b-curves for atomic cesium lines for a helium-cesium mixture. Seeding ratio $a = 10^{-2}$, Total pressure = 1 atmosphere

and the fundamental expression b by [see Equation (15)]:

$$b = \log \left\{ \frac{\dfrac{P}{2kT_1} + \phi(T_1)\left[1 - \sqrt{1 + \dfrac{P}{\phi(T_1)kT_1}}\right]}{\dfrac{P}{2kT_2} + \phi(T_2)\left[1 - \sqrt{1 + \dfrac{P}{\phi(T_2)kT_2}}\right]} \times \frac{u(T_2)}{u(T_1)} \right\}$$ (28)

$$T_2 \equiv \frac{T_1}{1 - aT_1}$$

The maximum errors in a and b due to the measuring errors of ΔY_n^m, ΔY_q^p and E_m, E_p are given by the relation [see Equations (22) and (23)]:

$$\Delta a = \pm \frac{k \ln 10}{|E_p - E_m|} \left[\left|\Delta(\Delta Y_n^m)\right| + \left|\Delta(\Delta Y_q^p)\right| + \left|\frac{\Delta Y_q^p - \Delta Y_n^m}{E_p - E_m}\right| \cdot \left(\left|\Delta E_m\right| + \left|\Delta E_p\right|\right) \right]$$ (29)

$$\Delta b = \pm \frac{1}{|E_p - E_m|} \left[E_m\left|\Delta(\Delta Y_q^p)\right| + E_p\left|\Delta(\Delta Y_n^m)\right| + \left|\frac{\Delta Y_q^p - \Delta Y_n^m}{E_p - E_m}\right| \cdot \left(E_m\left|\Delta E_p\right| + E_p\left|\Delta E_m\right|\right) \right]$$ (30)

Evaluating the total differential of Equation (28) with respect to a, b, T_1, and replacing the differentials by the corresponding erros, the theoretical relation between the errors Δa, Δb and ΔT_1 and ΔP is obtained. From this relation, the maximum relative error $\Delta T_1/T_1$ in temperature and the maximum relative error $\Delta P/P$ in pressure are derived as:

$$\frac{\Delta T_1}{T_1} = \pm \frac{\ln 10 \left|\Delta b\right| + \Pi(P, T_1, a)\left|\dfrac{\Delta P}{P}\right| + \psi(P, T_1, a)\dfrac{T_1}{|1 - aT_1|}\left|\Delta a\right|}{\theta(P, T_1, a)}$$ (31)

$$\frac{\Delta P}{P} = \pm \frac{\ln 10 \left|\Delta b\right| + \theta(P, T_1, a)\left|\dfrac{\Delta T_1}{T_1}\right| + \psi(P, T_1, a)\dfrac{T_1}{|1 - aT_1|}\left|\Delta a\right|}{\Pi(P, T_1, a)}$$ (32)

where, with $T_2 \equiv \dfrac{T_1}{1 - aT_1}$:

$$\Pi(P, T_1, a) = \left| \frac{P}{2kT_1}\left[1 - \frac{1}{\sqrt{1 + \dfrac{P}{\phi(T_1)kT_1}}}\right] N^{-1}(P, T) - \frac{P}{2kT_2}\left[1 - \frac{1}{\sqrt{1 + \dfrac{P}{\phi(T_2)kT_2}}}\right] N^{-1}(P, T_2) \right|$$

$$\psi(P, T_1, a) = \left| \frac{\overline{X}(T_2)}{kT_2} + \left\{ \frac{P}{2kT_2} \left[1 - \frac{1}{\sqrt{1 + \dfrac{P}{\phi(T_2)kT_2}}} \right] - \right. \right.$$

$$\left. \left. \phi(T_2) \left[\frac{3}{2} + \frac{W + \overline{X^+}(T_2) - \overline{X}(T_2)}{kT_2} \right] \cdot \left[1 - \frac{1 + \dfrac{P}{2\phi(T_2)kT_2}}{\sqrt{1 + \dfrac{P}{\phi(T_2)kT_2}}} \right] \right\} N^{-1}(P, T_2) \right|$$

$$\theta(P, T_1, a) = \left| \frac{\overline{X}(T_1) - \overline{X}(T_2)}{kT_1} + \left\{ \frac{P}{2kT_1} \left[1 - \frac{1}{\sqrt{1 + \dfrac{P}{\phi(T_1)kT_1}}} \right] - \right. \right.$$

$$\left. \phi(T_1) \left[\frac{3}{2} + \frac{W + \overline{X^+}(T_1) - \overline{X}(T_1)}{kT_1} \right] \cdot \left[1 - \frac{1 + \dfrac{P}{2\phi(T_1)kT_1}}{\sqrt{1 + \dfrac{P}{\phi(T_1)kT_1}}} \right] \right\} N^{-1}(P, T_1) -$$

$$\frac{T_2}{T_1} \left\{ \frac{P}{2kT_2} \left[1 - \frac{1}{\sqrt{1 + \dfrac{P}{\phi(T_2)kT_2}}} \right] - \right.$$

$$\left. \left. - \phi(T_2) \left[\frac{3}{2} + \frac{W + \overline{X^+}(T_2) - \overline{X}(T_2)}{kT_2} \right] \cdot \left[1 - \frac{1 + \dfrac{P}{2\phi(T_2)kT_2}}{\sqrt{1 + \dfrac{P}{\phi(T_2)kT_2}}} \right] \right\} N^{-1}(P, T_2) \right|$$

(33)

$$\overline{X}(T) = \frac{\displaystyle\sum_{s=0}^{\infty} g_s x_s e^{-\frac{x_s}{kT}}}{\displaystyle\sum_{s=0}^{\infty} g_s e^{-\frac{x_s}{kT}}} \, , \quad \overline{X^+}(T) = \frac{\displaystyle\sum_{s=0}^{\infty} g_s^+ x_s^+ e^{-\frac{x_s^+}{kT}}}{\displaystyle\sum_{s=0}^{\infty} g_s^+ e^{-\frac{x_s^+}{kT}}}$$

$$N(P, T) = \frac{P}{2kT} + \phi(T) \left[1 - \sqrt{1 + \frac{P}{\phi(T)kT}} \right]$$

Equations (31) and (32) give the relative error $\Delta T_1/T_1$ of the temperature measurement and the relative error $\Delta P/P$ of the pressure measurement as function of P, T_1, a and the corresponding measuring errors $\{\Delta a,\ \Delta b,\ \Delta P\}$ and $\{\Delta a,\ \Delta b,\ \Delta T_1\}$, respectively. Thus, by estimating the measuring errors, the error in the measuring result (i.e., the exactness of the method) in the respective region of P, T, and a can be precalculated.

Numerical investigation of the error relations, Equations (31) and (32), show that the method can be used with a considerable degree of accuracy $[(\Delta T_1/T_1)\ 100 < 10\%;\ (\Delta P/P)\ 100 < 10\%]$, if the plasma temperature or plasma pressure lies in that temperature or pressure region, respectively, where the theoretical b versus T_1 curve (temperature measurement) or theoretical b versus P curve (pressure measurement) is changing rapidly. Furthermore, it is found that the method is the more accurate the larger the experimentally observed a- parameter is — i.e., the more different the temperatures of the compared spectral lines are. However, it has to be considered that at very high a- values, the plasma pressure can only be assumed to be approximately constant. In this connection, it is remarkable that the temperature measurement is not very sensitive to small uncertainties in the plasma pressure.

With regard to a 1% cesium seeded helium plasma at atmospheric pressure, the method is restricted to a temperature region between $T_1 \cong 2000$ to 5000°K. This is exactly the region of tne electron temperature within which MPD energy conversion becomes of practical interest.

Calculation and Measurement of the Radial Distribution
of Line Broadening in a Cesium Plasma

In MPD power generation devices as well as in thermionic energy converters, the plasma properties change (in general) rapidly within the electrode sheaths and boundary layers. Therefore, a method for the determination of electron density in nonuniform plasmas is desirable. One such method for determination of the electron density is based on the line broadening caused by the Stark effect. In the case of cesium, which has been used in both MPD power generators and thermionic converters, this method has been applied successfully by several investigators.[8,9] Theoretical calculations of the line width for cesium have been made by Griem,[10] Agnew, and Summers.[11]

In the interpretation of spectrum it must be recognized that the observed radiation comes from different plasma layers, where different electron densities are present. Therefore, the line width observed on the photographic plate may be a mixture of a large number of differing line widths. In the case of a cylindrical plasma configuration it is possible to separate this mixture. This procedure is described later in this subsection.

In addition to determining the true line width rather than an averaged value, this procedure allows several line widths corresponding to the electron density profile of the discharge to be obtained through the analysis of a single line. This is extremely important in applications which allow a short running time and necessitate a maximum of information for each single exposure.

MATHEMATICAL METHOD

The problem of determining the true intensity is due to the fact that a cylindrical gas discharge usually has a temperature and density profile and, therefore, does not radiate uniformly. This problem has been approached and solved for the case of continuous and line radiation, neglecting broadening, by Hörmann,[2] Maecker,[3] and Pierce.[12] The resulting solutions have been used by many other investigators.

To obtain the true distribution of intensity within the discharge, it is necessary to consider the Abel integral equation. This equation is based on the transformation of intensity from cartesian to cylindrical coordinates:

$$x^2 + y^2 = r^2$$

In differential form, this equation becomes $\dfrac{dy}{dr} = \dfrac{r}{\sqrt{r^2 - x^2}}$

The intensity at any point x, y is related to the intensity density i(r) by

$$d\,I_{x,\,y} = i(r)\,dy$$

It follows that: $d\,I_{x,\,y} = i(r)\dfrac{r\,dr}{\sqrt{r^2 - x^2}}$

Integration of the expression between the limits r = x and r = R results in:

$$I(x) = 2\int_{r=x}^{R} d\,I_{x,\,y} = 2\int_{r=x}^{R} i(r)\,\dfrac{r\,dr}{\sqrt{r^2 - x^2}}$$

A factor of 2 has been added in the last expression to include both halves of the cylinder.

Figure 11 illustrates the usual approach for solution of this equation by numerical integration. The notation is after Pierce.[11] In Figure 11, the emitting volume is assumed to be a uniformly thick slab with cylindrical geometry. The density of the emitter is assumed to be a step function of the radius rather than a continuous function. The intensity density, assuming a thickness of unity, of the segment (j, k) becomes:

$$i_{(j,\,k)} = \dfrac{I_j}{2\Delta A_{j,\,k}}\,,\ \text{where } I_j \text{ is the observed intensity.}$$

The notation indicates an axial location j and radial location k. Since the discharge may be considered as axisymmetrical, the intensity of the outer ring (Figure 11) becomes

$$i_k = i_{(j,\,k)} = \dfrac{I_j}{2\Delta A_{j,\,k}}$$

The intensity density of the second ring referenced from the outer diameter (Figure 11) may be found by subtraction of the radiated energy of the outer ring from the observed intensity at position j-1. Therefore,

$$i_{k-1} = \dfrac{I_{j-1} - 2i_k\Delta A_{j-1,\,k}}{2\Delta A_{j-1,\,k-1}}$$

26
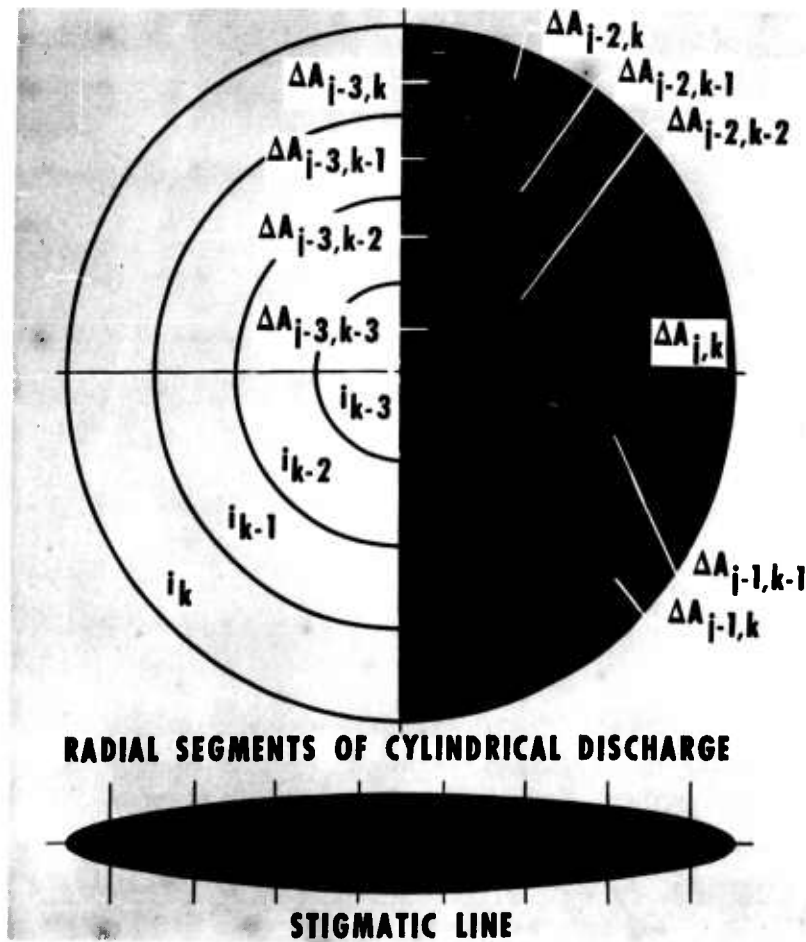
Figure 11. Numerical integration.

As progression is made toward the center of the discharge, the intensity density within each incremental ring may be found. The intensity densities of each radial increment multiplied by the respective transverse areas are used to calculate the intensity density in the next smaller ring. By selecting small increments the procedure provides a profile which approaches the true radial distribution of intensity density. The series expression for this computation becomes:

$$i_{k-n} = \frac{I_{j-n} - 2\Delta A_{j-n,\ k-(n-1)} - 2\Delta A_{j-n,\ k-(n-2)} - \cdots - 2\Delta A_{j-n,\ k}}{2\Delta A_{j-n,\ k-n}}$$

where n = 1, 2, 3, 4, ...

Each incremental area as illustrated in Figure 11 may be computed by [12]

$$\Delta A_{j,\,k} = \frac{1}{2}\left[r_k^2 \left(\theta_{j-1,\,k} - \theta_{j,\,k}\right) - r_{k-1}^2 \left(\theta_{j-1,\,k-1} - \theta_{j,\,k-1}\right) + \right.$$

$$\left. x_j \left(y_{j,\,k} - y_{j,\,k-1}\right) - x_{j-1}\left(y_{j-1,\,k} - y_{j-1,\,k-1}\right)\right]$$

where

$$\theta = \cos^{-1}\frac{x_j}{r_j}$$

and

$$y = r_k \sin\theta$$

The foregoing procedure converts an experimentally obtained intensity-versus-x-distribution in an intensity-density-versus-r-distribution. This procedure can be applied either on continuous radiation or on line radiation without broadening.

In order to take into account the broadening, the procedure becomes more complicated. Figure 12 is a schematic of the computational procedure. Figure 12a is a sketch of a typical line of an observed stigmatic spectrum. The line is normally more broadened in the inside than in the outer zones where the electron density gradually goes to zero. This, however, is not always true—e. g., in high temperature plasmas lines with a torus-like shape have been observed. The line, regardless of its shape, is divided in ten zones as indicated in Figure 12a. After scanning with a microdensitometer, a family of traces of photographic density versus d is obtained (Figure 12b).

In the next step the photographic density is converted into intensity by the relation:

$$D = \gamma \log I$$

D = spectrum density
I = intensity
γ = gamma function of photographic plate
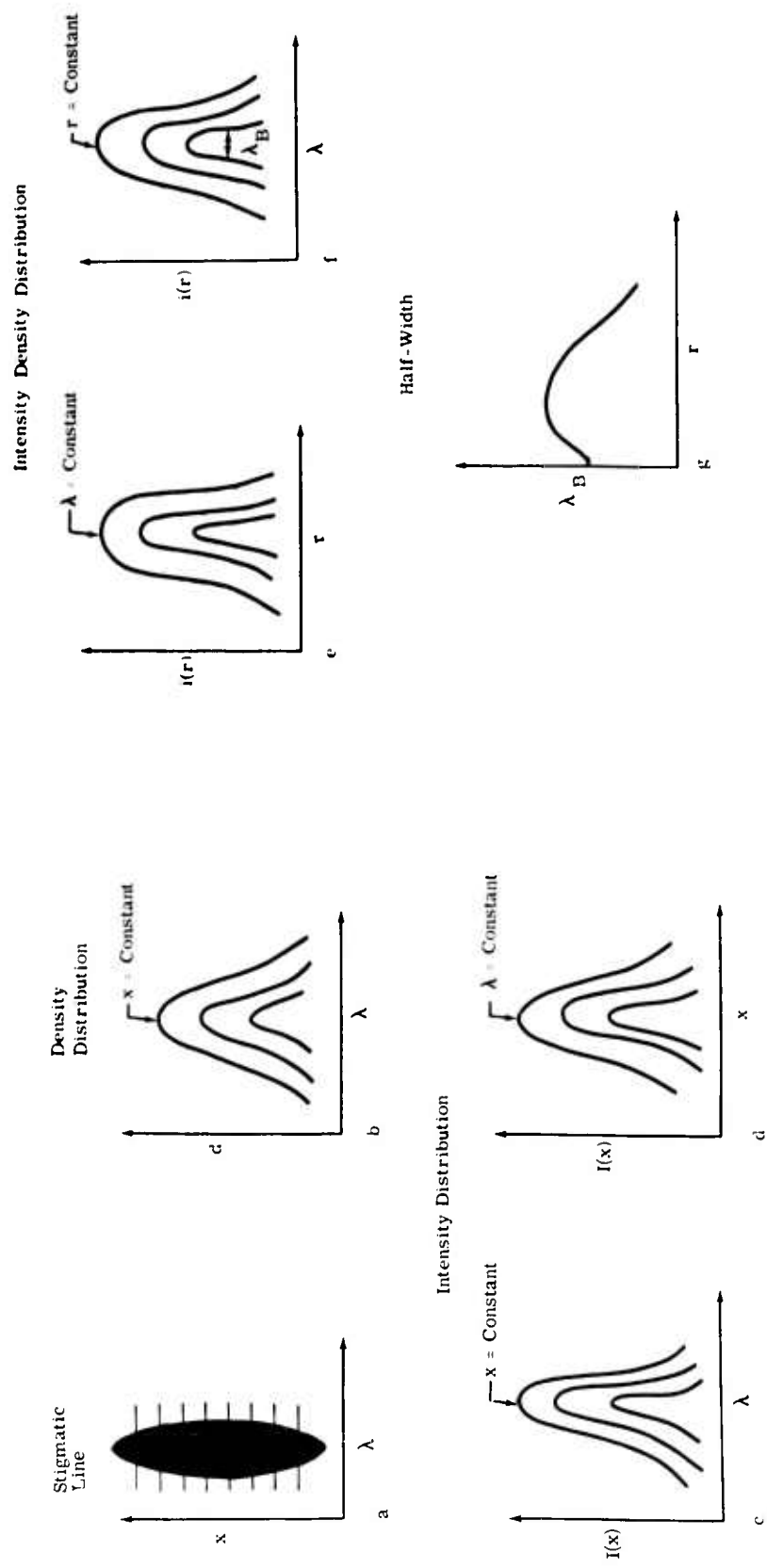
Figure 12. Line broadening calculation.

29

Since this relation holds only in the density range 0.8-1.8, in this application it is necessary to use Seidel's transformation,

$$W = \log \left(\frac{1}{T} - 1\right)$$

to convert Figure 12b to Figure 12c.

T is related to D by:

$$D = \log \frac{1}{T}$$

The family of curves obtained in Figure 12c is now an intensity-versus-λ-distribution with x as parameter.

The next step is to transform this into a family of curves with x as ordinate and λ as parameter. This change of variables is accomplished by reading in all the x's for a given λ. This procedure is a common computer problem and, therefore, will not be described further here. Now, the conventional Abel transformation, already described, is applied in going from Figure 12d to Figure 12e. A family of curves is now obtained which gives an intensity-density-versus-r distribution with λ as parameter.

To go from Figure 12e to Figure 12f, again a change of variables has to be made. For a certain r all the different λ values are read in and a family of curves, intensity-density-versus-λ, is obtained. Thus, the mixture of all the different line shapes, which originally existed, is separated into its components. The last step is to plot the half width of the lines versus r (Figure 12g). Using the results of Griem[10] or Agnew and Summers,[11] this plot can be converted into an electron density profile.

APPLICATION

The numerical procedure has been applied to line broadening measurements of a cesium diode, the spectrum of which has been taken with an Ebert 3.4-meter grating spectrograph. Data have also been obtained with respect to line broadening of helium in an arc discharge. The true distribution of half width (width at one-half maximum intensity) is compared with the distribution obtained from the observed stigmatic spectrum (Figure 13).
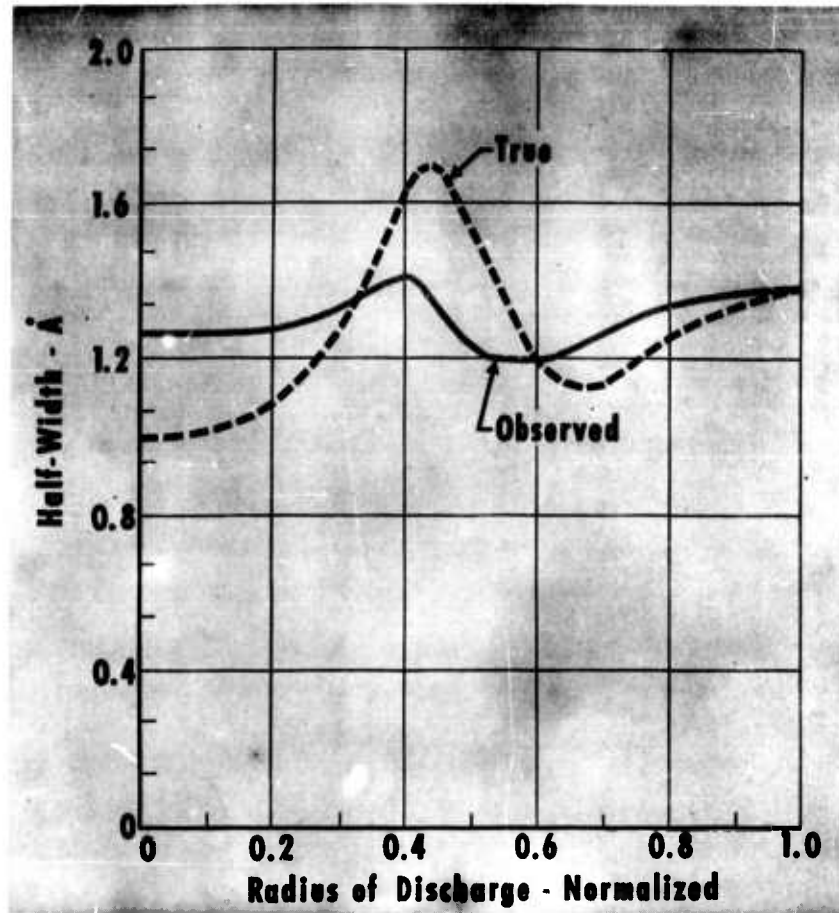
Figure 13. Radial distribution of half-width $\lambda = 6629$ Å.

In order to ensure independence of nonequilibrium effects, the fundamental series line, 6629 A, has been isolated for the analysis. Note from Figure 13 that the observed distribution tends to give an average of the true distribution.

The distribution of half width has been converted to the radial distribution of electron density according to the relation presented by Agnew and Summers,

$$\lambda_B = 2^{n-5} \times 1.5 \, N_e \times 10^{-15}$$

For the fundamental series transitions, 5D-nF for $5 \leqslant n \leqslant 8$, the line broadening has been estimated to be independent of electron temperature over a temperature range of 2000°K to 10,000°K. Since n = 8 for the 6629 A line, the electron density is expressed as:

$$N_e = \frac{\lambda_B}{12} \times 10^{15} \, \frac{electrons}{cm^3}$$

31

By applying this equation, the radial distribution of electron density as shown in Figure 14 is obtained. The electron density is low in the center of the discharge where the temperature is maximum. For this type of discharge, the partial pressure ($P_e = N_e k T_e$) tends to remain constant. As the temperature decreases, the electron density increases until a point is reached where the temperature is sufficiently low that ionization becomes negligible. Thus, the electron density starts to decrease. The rise of electron density at the outer radial zones is probably due to the back currents in the walls of the plasma container.

This method allows a detailed investigation of radial distribution of electron density. Because the stigmatic line spectrum does not allow precise determination of the location of the electron distribution within the discharge, the method is used in conjunction with the Spectrum Picture Method discussed in the First Quarterly Technical Summary Report, EDR 3155.
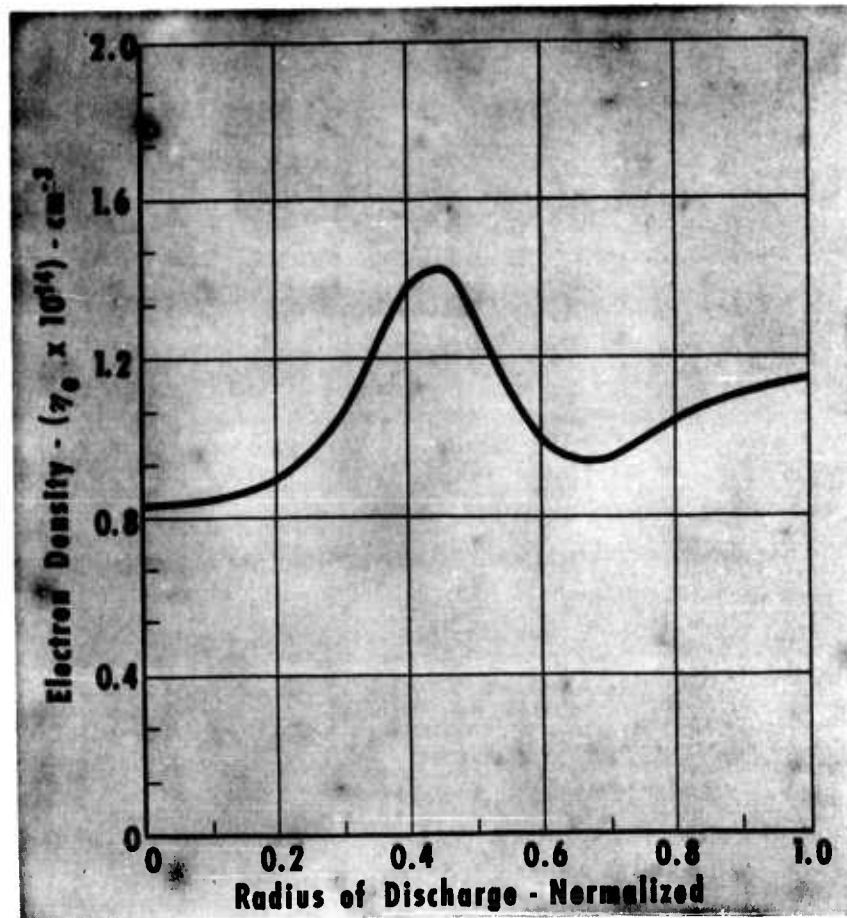
Figure 14. Radial distribution of electron density.

V. THEORETICAL PLASMA PROPERTIES

The computations of the properties of cesium-seeded helium plasma, Tables I and II and Figure 15, were carried through by consideration of the ionization of cesium and helium. The theoretical relations used are given in Equations (1), (6), (10) through (14), and (26). The ionization potentials were corrected for the depression by the electrostatic microfield and the Debye polarization. The main assumptions are distribution of the excited states according to Boltzmann statistics and existence of local thermodynamic equilibrium. The variables considered were:

Temperature, T = 1000 to 15,000°K

Seeding Ratio, α = 10^{-2}

Pressure, P = 1 atmosphere

Table I.
Particle densities.

Seeding ratio: $\alpha = 10^{-2}$

T—°K	n_-—cm^{-3}	n_{He}—cm^{-3}	n_{He}^+—cm^{-3}	n_{Cs}^+—cm^{-3}	n_{Cs}—cm^{-3}
0.09999999E 04	0.87237969E 09	0.72663204E 19	0.	0.87237967E 09	0.72663201E 17
0.11000000E 04	0.64319668E 10	0.66057462E 19	0.	0.64319666E 10	0.66057454E 17
0.12000000E 04	0.34056418E 11	0.60552672E 19	0.	0.34056417E 11	0.60552637E 17
0.13000000E 04	0.13976138E 12	0.55894773E 19	0.	0.13976138E 12	0.55894633E 17
0.13999999E 04	0.46943051E 12	0.51902287E 19	0.	0.46543050E 12	0.51901817E 17
0.15000000E 04	0.13431007E 13	0.48442124E 19	0.	0.13431007E 13	0.48440780E 17
0.16000000E 04	0.33730175E 13	0.45414471E 19	0.	0.33730175E 13	0.45411097E 17
0.16999999E 04	0.76077510E 13	0.42742987E 19	0.	0.76077507E 13	0.42753578E 17
0.18000000E 04	0.15687730E 14	0.40368292E 19	0.	0.15687729E 14	0.40352604E 17
0.19000000E 04	0.29993778E 14	0.38243496E 19	0.	0.29993777E 14	0.38215502E 17
0.20000000E 04	0.53769908E 14	0.36331072E 19	0.	0.53769907E 14	0.36277301E 17
0.25000000E 04	0.49366184E 15	0.29060395E 19	0.	0.49366183E 15	0.28566733E 17
0.30000000E 04	0.21044403E 16	0.24200233E 19	0.	0.21044403E 16	0.22095793E 17
0.34999999E 04	0.54531532E 16	0.20706925E 19	0.49782658E-11	0.54531531E 16	0.15253771E 17
0.40000000E 04	0.95690215E 16	0.18071059E 19	0.75566964E-07	0.95690212E 16	0.85020377E 16
0.45000000E 04	0.12277472E 17	0.16025820E 19	0.16407625E-03	0.12277472E 17	0.37483484E 16
0.50000000E 04	0.12921084E 17	0.14404710E 19	0.89429127E-01	0.12921084E 17	0.14836254E 16
0.59999999E 04	0.11706611E 17	0.11994627E 19	0.13742152E 04	0.11706610E 17	0.28801613E 15
0.70000000E 04	0.10190389E 17	0.10279562E 19	0.14569885E 07	0.10190389E 17	0.89172329E 14
0.80000000E 04	0.89554995E 16	0.89942219E 18	0.28012296E 09	0.89554991E 16	0.38722748E 14
0.90000000E 04	0.79740614E 16	0.79947068E 18	0.17120475E 11	0.79740444E 16	0.20662419E 14
0.09999999E 05	0.71828121E 16	0.71948466E 18	0.46763553E 12	0.71823445E 16	0.12506811E 14
0.11000000E 05	0.65369049E 16	0.65379582E 18	0.70914647E 13	0.65298133E 16	0.82156769E 13
0.12000000E 05	0.60551912E 16	0.59917856E 18	0.68466927E 14	0.59867042E 16	0.57661821E 13
0.13000000E 05	0.59680735E 16	0.55234339E 18	0.44464715E 15	0.55234262E 16	0.44539829E 13
0.13999999E 05	0.69789090E 16	0.51009224E 18	0.18635305E 16	0.51153784E 16	0.41792256E 13
0.15000000E 05	0.99082298E 16	0.46937503E 18	0.51676381E 16	0.47405914E 16	0.48350810E 13

Legend:

n_- = electron density

n_{Cs}^+ = cesium ion density

n_{He}^+ = helium ion density

n_{Cs} = cesium atom density

n_{He} = helium atom density

Pressure = 1 atmosphere

Table II.

Atomic partition functions.

T—°K	u_{Cs}	u_{He}
0.09999999E 04	0.20000003E 01	0.09999999E 01
0.11000000E 04	0.20000017E 01	0.09999999E 01
0.12000000E 04	0.20000063E 01	0.09999999E 01
0.13000000E 04	0.20000187E 01	0.09999999E 01
0.13999999E 04	0.20000470E 01	0.09999999E 01
0.15000000E 04	0.20001049E 01	0.09999999E 01
0.16000000E 04	0.20002123E 01	0.09999999E 01
0.16999999E 04	0.20003967E 01	0.09999999E 01
0.18000000E 04	0.20006930E 01	0.09999999E 01
0.19000000E 04	0.20011444E 01	0.09999999E 01
0.20000000E 04	0.20018011E 01	0.09999999E 01
0.25000000E 04	0.20103406E 01	0.09999999E 01
0.30000000E 04	0.20343957E 01	0.09999999E 01
0.34999999E 04	0.20845613E 01	0.09999999E 01
0.40000000E 04	0.21741723E 01	0.09999999E 01
0.45000000E 04	0.23214344E 01	0.09999999E 01
0.50000000E 04	0.25504491E 01	0.09999999E 01
0.59999999E 04	0.33720669E 01	0.09999999E 01
0.70000000E 04	0.48827805E 01	0.09999999E 01
0.80000000E 04	0.72842665E 01	0.09999999E 01
0.90000000E 04	0.10693043E 02	0.09999999E 01
0.09999999E 05	0.15137806E 02	0.09999999E 01
0.11000000E 05	0.20578072E 02	0.09999999E 01
0.12000000E 05	0.26927919E 02	0.09999999E 01
0.13000000E 05	0.34076749E 02	0.10000001E 01
0.13999999E 05	0.41904649E 02	0.10000013E 01
0.15000000E 05	0.50292623E 02	0.10000070E 01

u_{Cs} = partition function of Cs

u_{He} = partition function of He

35
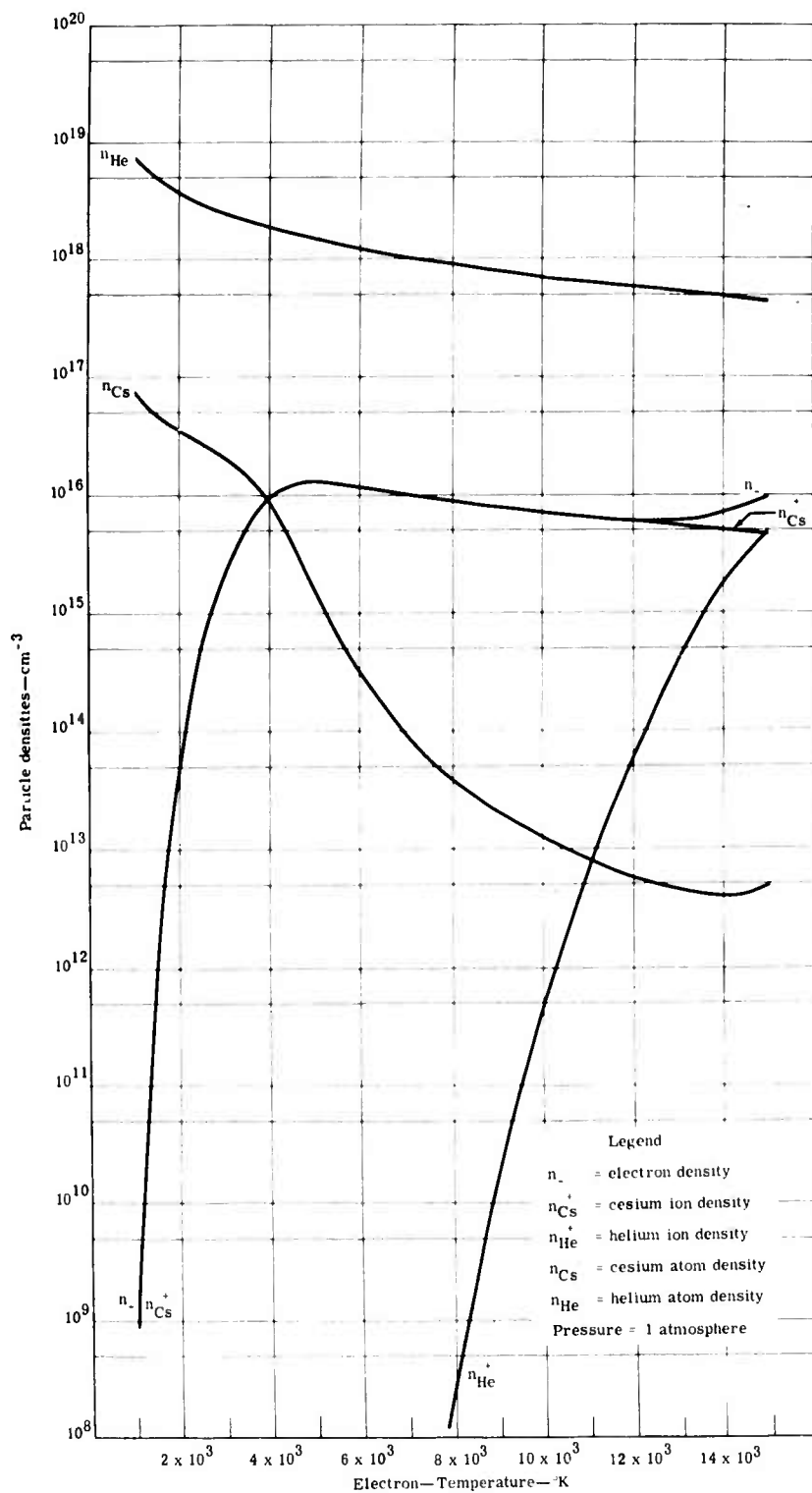
Figure 15. Particle densities in cesium-seeded helium plasma.

VI. BIBLIOGRAPHY

1. Ornstein, L. S. and Brinkmann, H. Physica 1, 797 (1934).

2. Hoermann, H., in Zeitschr. f. Physik 97, 539 (1935).

3. Maecker, H., in Zeitschr. f. Physik 136, 119 (1953).

4. Fowler, R. H. and Milne, E. A. Statistical Mechanics. Cambridge, (1936).

5. Larenz, H., in Zeitschr. f. Physik 129, 327 (1951).

6. Bartels, H. and Larenz, H., in Naturwiss. 37, 164 (1950).

7. Ecker, G. and Weizel, W., in Ann. Phys. 17, 126 (1956).

8. Stone, P. M. and Agnew, L. "Plasma Broadened Cesium Lines." Physics Review. Vol 127, No. 4 (August 1962).

9. Donahuc, R. J. and Majkowski, R., in Journal of Applied Physics 33, 3 (1963).

10. Griem, H. Plasma Spectroscopy. McGraw Hill, 1964.

11. Agnew, L. and Summers, C. "Experimental Cesium Line Shapes." Advanced Energy Conversion. Vol 3, Pergamon Press, 1963, pp 79-87.

12. Pierce, W. J. Conference on Extremely High Temperatures, Fischer and Mansur, ed. John Wiley & Sons, 1958, pp 123-34.

No. copies

Director, Advanced Research Projects Agency
The Pentagon
Washington, D. C. 20301
    Attn: Dr. John Huth   2

Office of Naval Research
Power Branch (Code 429)
Washington, D. C. 20360
    Attn: John A. Satkowski   6

Commanding Officer
Office of Naval Research Branch Office
Box 39 Navy #100 Fleet Post Office
New York, New York   1

Cognizant ONR Area Branch Office   1

U. S. Naval Research Laboratory
Washington 25, D. C.
    Attn: Technical Information Division   6

Wright-Patterson Air Force Base
Aeronautical Systems Division
Ohio
    Attn: Don Warnock (ASRMFP-2)   1

Air Force Office of Scientific Research
Washington 25, D. C.
    Attn: Dr. Milton M. Slawsky   1

U. S. Naval Ordnance Test Station
Propulsion Applied Research Group
China Lake, California
    Attn: Leroy J. Krzycki (Code 4506)   1

Rome Air Development Center
Rome, New York
    Attn: Mr. Frank J. Mellura   1

U. S. Naval Ordnance Laboratory
NA Division
White Oak, Maryland
    Attn: Wallace Knutsen   1
          Library   2

Defense Documentation Center
Cameron Street
Alexandria, Virginia 22314   20

U. S. Army Research & Development Laboratory
Fort Belvoir, Virginia
    Attn: Frank Shields (ERD-EP)   1

NASA, Lewis Research Center
21,000 Brookpark Road
Cleveland 35, Ohio
    Attn: Wolfgang Moeckel   1
         Dr. B. Lubarsky   1

U. S. Atomic Energy Commission
Division of Reactor Development
Direct Energy Conversion Section, RD; AED
Germantown, Maryland   1

Dr. T. Brogan
AVCO - Everett Research Laboratory
2385 Revere Beach Parkway
Everett, Massachusetts   1

Dr. J. Cole
Department of Aeronautics
California Institute of Technology
Pasadena, California   1

Mr. Arthur Sherman
General Electric - Valley Forge
Valley Forge Space Technical Center
Philadelphia 1, Pennsylvania   1

Dr. M. Talaat
Martin Marietta Corporation
Nuclear Division
Baltimore 3, Maryland   1

Dr. W. D. Jackson
Electrical Engineering Department
Massachusetts Institute of Technology
Cambridge 39, Massachusetts   1

Dr. Vernon H. Blackman
MHD Research Incorporated
1535 Monrovia Street
Newport Beach, California   1

Dr. B. C. Lindley
Nuclear Research Centre
C. A. Parsons & Co., Ltd.
Fossway, Newcastle Upon Tyne 6
England   1

Dr. Robert Eustis
Thermosciences Divsion
Stanford University
Standford, California   1

Mr. John Wright
Central Electricity Research Laboratories
Cleeve Road, Leatherhead, Surrey
England   1

Dr. Richard Schamberg
Rand Corporation
1700 S. Main Street
Santa Monica, California   1

Dr. Sam Naiditch
Unified Science Associates
826 Arroyo Parkway
Pasadena, California   1

Dr. W. S. Emmerich
Westinghouse Research Laboratories
Beulah Road, Churchill Borough
Pittsburgh 35, Pennsylvania   1

Dr. R. T. Schneider
Allison Division
General Motors Corporation
Indianapolis, Indiana   1

Dr. D. G. Elliott
Jet Propulsion Laboratory
Pasadena, California   1